Melting of Ordered Arrays and Shape Transitions in Highly Concentrated Diblock Copolymer Solutions

Glen A. McConnell[†] and Alice P. Gast*

Department of Chemical Engineering, Stanford University, Stanford, California 94305-5025

Received August 15, 1996; Revised Manuscript Received November 7, 1996[⊗]

ABSTRACT: Polystyrene/polyisoprene (PS/PI) diblocks suspended in decane serve as a model system for the investigation of highly concentrated diblock copolymer solutions. Bulk melts of PS/PI with no solvent exhibit ordered morphologies including lamellae, close-packed cylinders, etc. that depend on the block asymmetry. These same diblocks self-assemble in decane at low concentrations to form monodisperse, spherical micelles with a dense polystyrene core and a diffuse polyisoprene corona. Strongly interacting polymeric micelles, observed at modest polymer concentrations, order into cubic arrays that include both face-centered and body-centered cubic crystals depending on the length scale of the repulsion relative to the core dimension. These ordered morphologies of the melt and micellar crystals provide limiting reference states for the poorly understood high-concentration regime studied in this work. As we increase the polymer concentration, we observe a curious melting of the micellar crystals before the onset of anisotropy. Since the melting of the micellar crystal is not predicated upon shape transitions, we return to tethered-chain models of our spherical polymeric micelles to qualitatively describe the disordering process in terms of a loss of the osmotic pressure gradient between micelles. One system exhibits a reentrant disorder−order−disorder−order phase transition. Finally, the development of anisotropy in the scattering pattern is linked to shape transitions that develop as melt conditions are approached. We monitor the degree of anisotropy to estimate the concentration for the onset of these shape transitions.

1. Introduction

The microphase separation of melt diblocks is reasonably well understood.[1] Experiments by Bates and others clearly demonstrate the formation of ordered domains that include lamellae,[2−4] close-packed cylinders,[5,6] body-centered cubic structures,[7] and a gyroid phase.[8,9] Leibler provided a phase diagram for diblock melts largely consistent with these experimental results.[10] This phase behavior becomes more complicated if another component is added to the diblock melt. The most obvious example involves the addition of a homopolymer chemically identical to one of the blocks. This case has been studied by Thomas, Cohen, and others.[11−13] Adding a small molecule, like a solvent, has been investigated to a lesser extent. This situation is potentially more complicated because the solvent can be selective for one or both domains. Hashimoto and coworkers initiated a series of studies on diblocks in the presence of several solvents having varying affinities for each block,[14−18] underscoring the broad range of possibilities for such suspensions.

Studying diblocks in the presence of a solvent selective for one block is particularly intriguing because these diblocks will self-assemble to produce spherical micelles at modest polymer concentrations. Polystyrene/polyisoprene (PS/PI) diblocks serve as a model system for investigations of a strongly phase-separated melt. When these same PS/PI diblocks are suspended in decane, a solvent preferential for polyisoprene, they self-assemble to produce monodisperse, spherical micelles with a dense core of polystyrene and a diffuse corona of polyisoprene. The block asymmetry alters the thermodynamics of micellization, yielding micelles with differing internal architectures.[19] For example, PS/PI diblocks with a low degree of polymerization for the PS, relative to the PI block, form micelles with a small core radius and a larger, diffusive corona. By reversing the asymmetry, we produce micelles with a higher mean aggregation number, a subsequently larger core radius, and a comparatively smaller corona. Since the tethered-chain portion of the micelle, specifically the corona, regulates the interactions between micelles, we acquire an experimental means of tuning the length scale of the interaction potential. In our previous work identifying the phase behavior of these micellar suspensions,[20] we discovered that they undergo a disorder−order transition to form either face-centered or body-centered cubic crystals depending on the length scale of the repulsion relative to the core radius. We have sufficiently characterized these micelles[21] to allow us to apply self-consistent field models of tethered-chain systems[22−26] to understand the liquid structure and phase behavior. This study provided a reasonable scaling relation for the disorder−order transition in terms of the micellar corona thickness relative to the core radius as expressed in a semiquantitative phase diagram.[27]

Investigations of the phase behavior of these strongly interacting polymeric micelles complement knowledge about the melt structure, leaving a yet poorly understood intermediate region of highly concentrated diblock copolymers in a selective solvent. Although the ordered, melt morphologies of diblock copolymers have been studied and understood for some time, very little research has been directed at the phase behavior of highly concentrated diblock copolymer solutions. The pioneering efforts of Gallot[28,29] represent the foundation of such studies. Suspending polybutadiene/polystyrene diblocks in styrene monomer, subsequently polymerized to produce a complete polymer matrix, permitted the samples to be cross-sectioned and examined using transmission electron microscopy (TEM). Although Gallot's experiments illustrated the breakdown of the melt morphology at modest styrene concentrations, the experiments never identified the cubic, micellar crystalline phases described in our experiments. In addition, the polymerization step, while novel for the purposes of using TEM, can lead to nonequilibrium structures.

[†] Present address: Cabot Corp., 157 Concord Rd., Billerica, MA 01821-7001.

[⊗] Abstract published in *Advance ACS Abstracts,* January 1, 1997.

S0024-9297(96)01241-7 CCC: $14.00 © 1997 American Chemical Society

Still, the revolutionary work of Gallot motivates our own interest in studying concentrated polystyrene/polyisoprene diblock copolymers in decane at concentrations between the ordered, micellar crystals and the melt to elucidate the mechanisms for shape transitions as the melt morphology is approached.

We begin with a description of the experimental protocol implemented in these investigations. In particular, we explain the use of oscillatory shear on concentrated samples for our 2-D SAXS diffraction studies. A series of diffraction images are presented at various concentrations for five *d*-PS/PI systems with varying block asymmetry and degree of polymerization in decane to establish a trend in the global disordering of our micellar crystals prior to the onset of additional anisotropy in the diffraction images observed at advanced polymer concentrations. Since the loss of cubic order in the micellar crystal occurs before the onset of these shape transitions, we can understand the disorder−order−disorder process by appealing to the physics of tethered-chain systems. As a result, we return to the self-consistent field equations used to describe the interactions in our polymeric micelles to explain the disordering process that occurs as a result of increasing the polymer concentration. We find that as the micelles are concentrated, they reach a threshold where the local polymer concentration gradient in the polyisoprene layer is diminished. Since this concentration gradient is responsible for the effective pair potential, the loss of the gradient removes the driving force for the ordered structure and the crystal melts. Finally, from the scattering anisotropy, we infer the commencement of shape transitions corresponding to the disruption of the original micellar architecture.

2. Results

2.1. Experimental Considerations. Perdeuterated polystyrene/polyisoprene (*d*-PS/PI) diblock copolymer samples[30] were suspended in decane at concentrations ranging from 12 to 85 wt %. The samples were initially dissolved in decane at concentrations of approximately 10 wt % in decane and placed in an oven at no more than 50 °C to aid dissolution. The samples were left uncapped in the oven under partial vacuum, and the excess decane was evaporated to achieve the desired concentration. This process took no more than 2 days, and the samples were subsequently allowed to equilibrate at room temperature for at least 3 days.

The experiments were performed at beamline 1-4[31] of the Stanford Synchrotron Radiation Laboratory (SSRL) using a recently commissioned X-ray area detector described below. Although contrast matching experiments are not possible, we still used a mixture of deuterated and hydrogenated decane as the solvent for consistency with previous neutron scattering experiments where a mole fraction of 0.107 *d*-decane provides a PI match scattering density. The use of this solvent mixture was a precautionary measure in order to remove the possibility of slight thermodynamic differences arising from deuteration.

We report investigations of five polystyrene/polyisoprene systems here: 15 000 molecular weight polystyrene and 15 000 molecular weight polyisoprene (15K/15K *d*-PS/PI), 19K/8K, 20K/10K, 45K/45K, and 36K/36K *d*-PS/PI diblocks in decane. These five systems represent a subset of eight PS/PI diblock systems investigated in the past to probe the phase behavior of polymeric micelles. We have previously characterized all these PS/PI micellar systems including dilute solution measurements of the hydrodynamic radius (R_h) from dynamic light scattering experiments and the core radius (R_c) from core-contrast SANS experiments.[20,21,32] The semiquantitative phase diagram for these polymeric micelles identifies the phase behavior observed for a polystyrene core volume fraction plotted as a function of the hydrodynamic coronal layer thickness ($\langle L\rangle_h = R_h - R_c$) relative to the the core radius. Table 1 offers the relevant micellar properties for each diblock system.

Table 1. Length Scales Describing Polymeric Micelles of *d*-PS/PI Diblocks in Decane

polymer	polydispersity	R_c (Å)	$\langle L\rangle_h$ (Å)
15K/15K	1.03	74	120
19K/8K	1.03	116	68
20K/10K	1.03	117	103
33K/22K	1.03	150	212
36K/36K	1.02	142	325
44K/22K	1.02	204	280
40K/40K	1.03	106	190
45K/45K	1.02	137	313

A hand-shearing device suitable for X-ray scattering experiments was constructed to act as the sample cell. Two independent Lexan sheets were machined to provide a gap of 1.5 mm. These Lexan sheets, the first being 1.5 × 1.5 in. and the second being 1.5 × 1 in., fit into an aluminum case allowing the smaller Lexan sheet to oscillate back and forth with a total pitch of 0.5 in. Samples were placed in this hand-shearing device and sheared with frequencies varying between 0.1 and 10 Hz with an amplitude that varied from 5 to 10 times the sample thickness. After preshearing the samples for several minutes, the samples were allowed to stand for 15 min before scattering so that the images represent at-rest diffraction images presheared to aid macroscopic ordering. The preparation of these samples in this manner produced at-rest diffraction images whose major axes correspond to a slice along the vorticity−velocity plane. The direction normal to this plane is parallel to the shear gradient, a direction coincident with the impinging X-rays. The aluminum case provided a free beam path for the X-rays such that the measured intensity includes contributions from the sample, the Lexan, and parasitic scattering only. Other shearing devices constructed from Lexan demonstrate that its contribution to the scattered intensity over this q range is negligible.[33,34]

These experiments were performed with a sample to detector distance of 1.0 m. The wavelength of the incident radiation equals 1.495 Å, and the flux was reduced to approximately 1×10^9 photons/s to minimize the parasitic scattering. We use an asymmetric beamstop of 3 × 5 mm because the mirror provides better focusing along the vertical direction. This arrangement gives an accessible range in the scattering vector q of 0.008−0.10 Å^{-1}, where $q = (4\pi/\lambda)\sin(\varphi/2)$. The detection and data acquisition included a CCD area "Olive" detector fabricated by Argonne National Labs and an external data bus all connected to a DEC Alpha computer. The active area of the detector is 1 in^2. Scattered X-rays impinge on a phosphorescent pad constructed of Gd_2O_2S:Tb (12 mg/cm^2), transforming the X-ray photons into a white light signal (at a gain of approximately 18 photoelectrons per every X-ray photon) carried along untapered fiber-optic lines to a standard charge-coupled device (CCD). This CCD (a Tektronix TK-1024 non-MPP front side illuminated device) is the same size as the phosphorescent pad, 1 × 1 in., divided into 1024

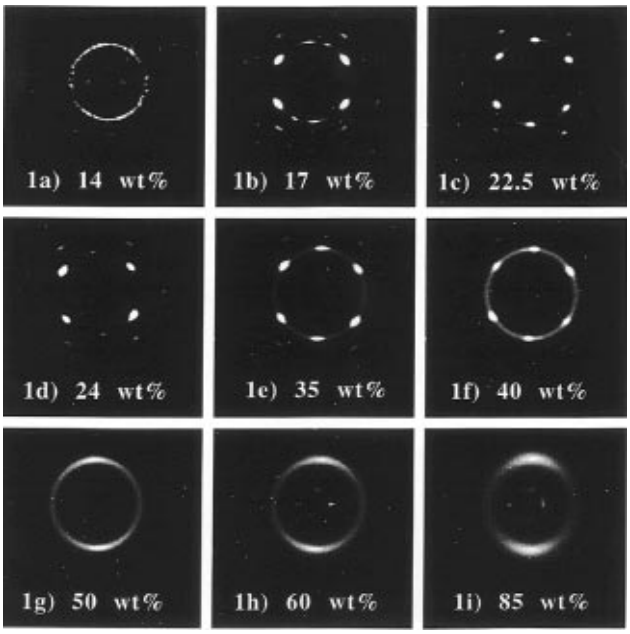

Figure 1. 2-D SAXS diffraction images for presheared 15K/15K *d*-PS/PI diblocks in decane at the following concentrations (in weight percent): (a) 14, (b) 17, (c) 22.5, (d) 24, (e) 35, (f) 40, (g) 50, (h) 60, and (i) 85.

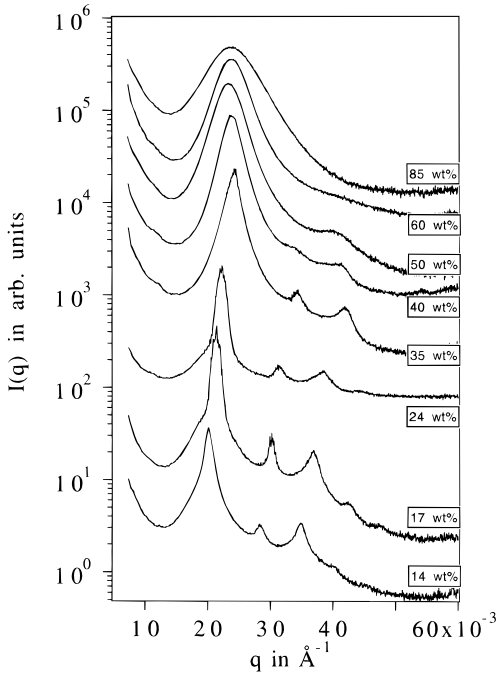

Figure 2. Radially averaged intensity profiles for the 15K/15K *d*-PS/PI diffraction images presented in Figure 1.

×1024 actual elements. At this stage, the signal is converted from a voltage difference to a 16-bit signal channeled to the external data bus. A complete diffraction image can be relayed in about 2 s, allowing rapid data acquisition for time-resolved studies. With binning or limited frame sizes, the transfer rate can approach tenths of a second; however, the experiments reported here are steady diffraction images integrated over several minutes. We reduced the data with routines developed by Stanton and co-workers for processing image sets.[35,36]

2.2. Scattering Images. The micelles formed from 15K/15K *d*-PS/PI diblocks in decane have a ratio of the hydrodynamic layer thickness to core radius $\langle L \rangle_h / R_c$ equaling 1.635. The phase diagram presented in Figure 12 shows that this system orders into a body-centered cubic (BCC) crystal at a core volume fraction of approximately $\Phi_{PS} = 0.06$. We prepared presheared samples ranging from 14 to 75 wt % polymer for structure determination by 2-D SAXS diffraction. These diffraction images are presented in Figure 1. The first diffraction image, labeled Figure 1a, offers the image taken for the 15K/15K *d*-PS/PI sample at 14 wt % in decane. Since this concentration is slightly below the initial ordering, the image is largely isotropic with speckles in the otherwise isotropic rings. At 17 wt %, Figure 1b, the image shows the twinned BCC structure identified in previous shear experiments on our micellar crystals as well as melt diblocks with a BCC morphology subjected to linear oscillatory shear.[7,32] This structure persists (Figures 1b−d) until we reach a concentration of 35 wt % where, we can see in the diffraction images presented in Figures 1d and 1e, the scattering includes an isotropic portion. This scattering can be interpreted as a superposition of ordered and disordered fractions; the disordered portion continues to increase as the concentration is increased to 40 wt % as illustrated in Figure 1f.

Ultimately all cubic order is lost and the scattering eventually develops into an anisotropic ring as the concentration is further increased. Figure 1g shows this anisotropic ring for the 15K/15K *d*-PS/PI sample at a total polymer concentration of 50 wt %. As we continue to increase the concentration, the diffraction images displayed in Figures 1h and 1i, corresponding to 60 and 85 wt % respectively, show an increase in the magnitude of the scattering vector *q* for the location of this ring as well a broadening of the line width. The increase in the magnitude of the scattering vector corresponds to a decrease in the separation distance between these structures as expected upon increasing the concentration. The line broadening may be related to the variability in the structures formed, suggesting a broad distribution of sizes in the structures leading to a range of spacings.

To appreciate this variability, we calculate and plot the radially averaged intensity in Figure 2. The intensities are plotted in arbitrary units and offset vertically for comparison. As described earlier, the sample at 50 wt % shows no sign of cubic structure. Interestingly, we are approaching the melt concentration for the 85 wt % sample without conclusive evidence for the melt morphology. The melt morphology for this 15K/15K *d*-PS/PI diblock system is a lamellar structure whose diffraction image gives a series of diffraction spots at even multiples defined by the lamellar spacing. Diffraction experiments by Bates[3] suggest that the lamellar ordering can be both parallel and perpendicular to the shear gradient; however, one cannot always resolve multiple diffraction spots for these systems. Given the unknown orientation of the system, we attempted to tilt our samples to probe the direction along the shear gradient. We were only able to achieve a 45° tilt angle and were not able to observe higher order diffraction peaks consistent with the lamellar morphology.

Two other systems, 19K/8K and 20K/10K *d*-PS/PI, form face-centered cubic (FCC) micellar crystals at modest polymer concentrations and have a melt morphology of hexagonally close-packed cylinders. We studied these diblocks in decane at concentrations ranging from 25 to 85 wt % in decane. The micelles comprising 19K/8K *d*-PS/PI diblocks are characterized

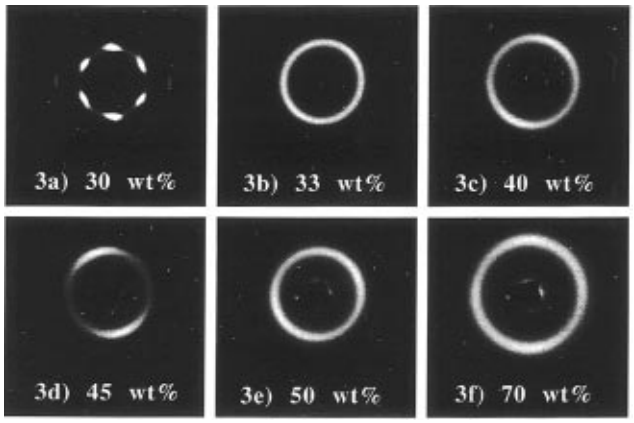

Figure 3. 2-D SAXS diffraction images for presheared 19K/8K *d*-PS/PI diblocks in decane at the following concentrations (in weight percent): (a) 30, (b) 33, (c) 40, (d) 45, (e) 50, and (f) 70.

with a coronal layer thickness to core radius of $\langle L \rangle_h / R_c = 0.586$, while the 20K/10K *d*-PS/PI micelles have a ratio of 0.88. The difference in the range of the repulsion for these two micellar systems leads to variations in the ordering core volume fraction. The 19K/8K *d*-PS/PI micelles order into an FCC crystal at a core volume fraction of approximately $\Phi_{PS} = 0.17$ while the 20K/10K *d*-PS/PI micelles order at a lower core volume fraction near 0.10.

The diffraction images presented in Figure 3 display the results for our investigations of the 19K/8K *d*-PS/PI system. At 25 wt % these micelles are ordered into a FCC crystal. The shear forces the crystal to flow in layers with the densest ⟨111⟩ planes stacked in the shear gradient. This produces a diffraction image (Figure 3a) from a 2-D hexagonally close-packed structure indicating the scattering from ⟨111⟩ planes with a stochastic stacking sequence for the two possible, threefold hollow sites available to the FCC micellar crystal.[32]

Unfortunately, the band of volume fractions giving an ordered FCC crystal for this system is quite narrow. At a polymer concentration of only 33 wt % (Figure 3b), the FCC micellar order is lost and the image shows a constant intensity ring with no scattering anisotropy. This isotropic structure persists up to a concentration of 40 wt %, where Figure 3 shows some anisotropy in the scattering that builds as we increase the concentration to 45 wt % (Figure 3d). We experience some experimental difficulties when we attempt to study this system at concentrations nearing the melt. As mentioned earlier, the melt morphology involves hexagonally close-packed cylinders of polyisoprene imbedded in a polystyrene matrix. Once we prepare the 19K/8K *d*-PS/PI diblocks at 70 wt %, as displayed in Figure 3f, the volume fraction of polystyrene for the sample begins to exceed one-half of the total sample volume fraction. This represents the point where the polystyrene becomes the major phase; here the sample is difficult to hand shear at room temperature. Despite these difficulties, we show this data because the magnitude of the *q* vector for this scattering ring has increased significantly. We show the radially averaged data for these same samples in Figure 4 to gain some appreciation for the variation in the scattering as a function of the scattering vector.

The 20K/10K *d*-PS/PI system shows a similar phenomenology, but the FCC micellar crystal region is much broader than it was in the 19K/8K *d*-PS/PI case. At 25 wt % (Figure 5a) we observe the typical FCC

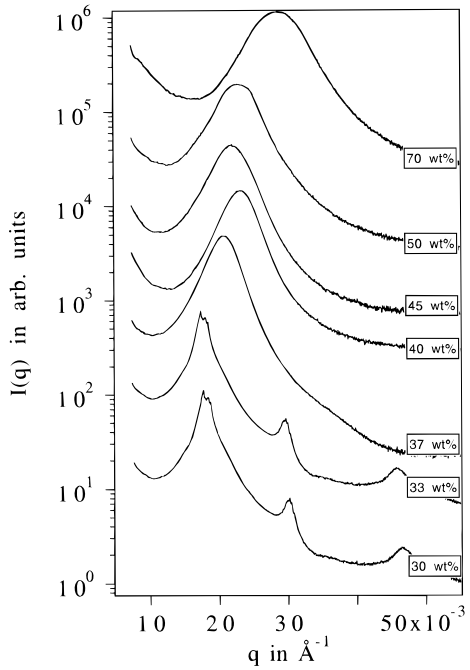

Figure 4. Radially averaged intensity profiles for the 19K/8K *d*-PS/PI diffraction images presented in Figure 3.

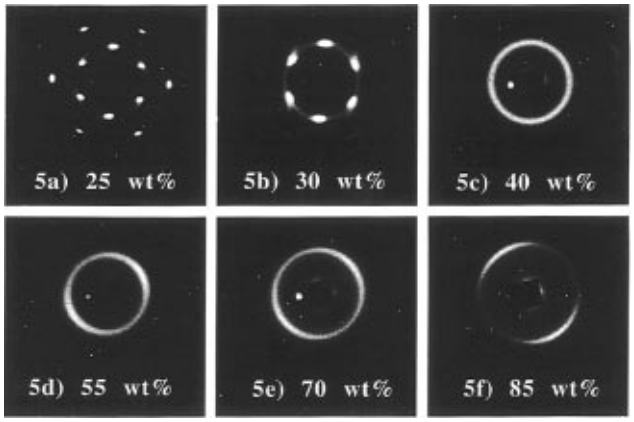

Figure 5. 2-D SAXS diffraction images for presheared 20K/10K *d*-PS/PI diblocks in decane at the following concentrations (in weight percent): (a) 25, (b) 30, (c) 40, (d) 55, (e) 70, and (f) 85.

diffraction image. Although the FCC image is maintained at 30 wt %, as displayed in Figure 5b, we begin to observe some destruction of the cubic structure and the onset of disordering with the development of the isotropic ring that is fully in evidence at 40 wt % (Figure 5c). As the concentration is increased to 55 wt %, we observe increased anisotropy in the ring. As we continue to increase the concentration, the anisotropy grows as does the magnitude of the scattering vector for the location of this ring. The change in the scattering intensity with respect to the magnitude of the scattering vector can also be seen in the radially averaged intensity profiles plotted in Figure 6.

In Figure 7 we present the results for our 45K/45K *d*-PS/PI diblocks in decane at concentrations ranging from 12 to 85 wt %. At 12 wt %, the sample shows the onset of the ordering transition for our 45K/45K *d*-PS/PI micelles. These micelles have a ratio of coronal layer thickness to core radius equaling 2.28. At 14 wt % (Figure 7b) we observe the diffraction pattern consistent with the formation of a BCC twin structure as expected for this sample. Surprisingly, we have a sudden loss of

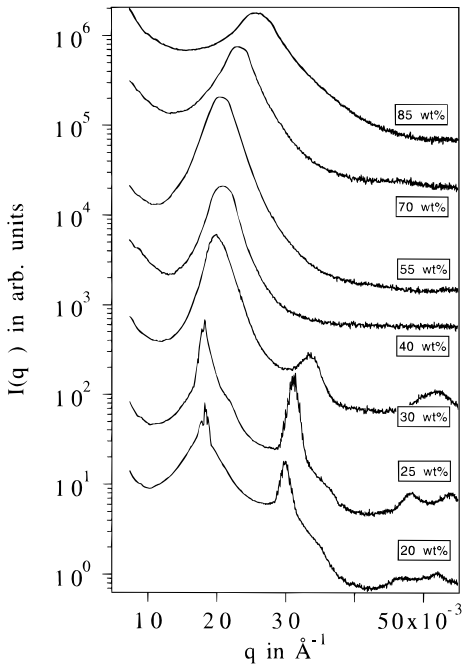

Figure 6. Radially averaged intensity profiles for the 20K/10K *d*-PS/PI diffraction images presented in Figure 5.

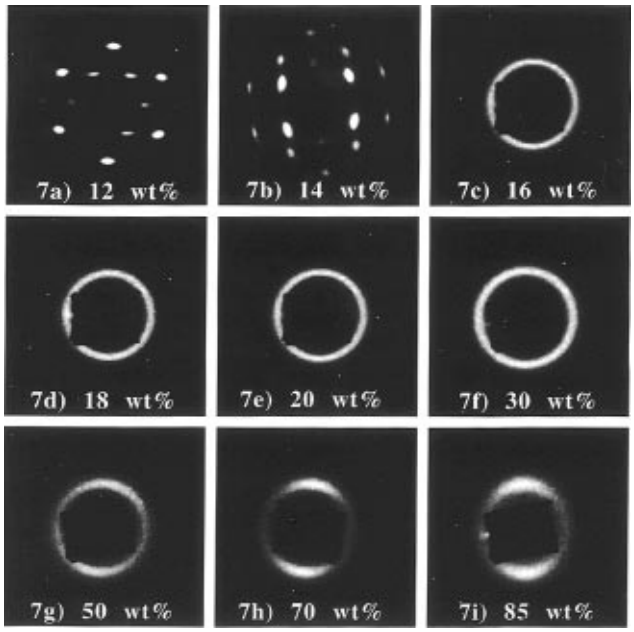

Figure 7. 2-D SAXS diffraction images for presheared 45K/45K *d*-PS/PI diblocks in decane at the following concentrations (in weight percent): (a) 12, (b) 14, (c) 16, (d) 18, (e) 20, (f) 30, (g) 50, (h) 70, and (i) 85.

cubic order at a concentration of only 16 wt % as seen in the isotropic ring displayed in Figure 7c. This isotropic, liquid-like, ring persists for concentrations ranging from 18 to 30 wt % (Figures 7d−f). At approximately 50 wt %, we finally observe the onset of some scattering anisotropy. This anisotropy continues to build as we increase the concentration to 85 wt % (Figure 7i).

Perhaps the most intriguing case involves the transitions experienced in the 36K/36K *d*-PS/PI diblock system shown in Figure 8. At 10 wt % (Figure 8a) we observe diffraction peaks suggesting an ordering transition. Powder diffraction from samples at this concentration suggest the formation of a body-centered-cubic crystal, but we are unable to conclusively identify the

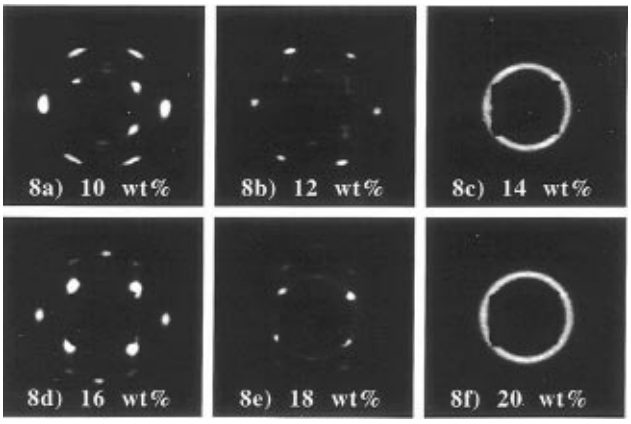

Figure 8. 2-D SAXS diffraction images for presheared 36K/36K *d*-PS/PI diblocks in decane at the following concentrations (in weight percent): (a) 10, (b) 12, (c) 14, (d) 16, (e) 18, and (f) 20.

phase at this concentration. In fact, scattering at 12 wt % (Figure 8b) shows some splitting of the diffraction spots for the innermost ring. While the diffraction spots imply the formation of an ordered structure, this long-range order suddenly disappears at 14 wt % (Figure 8c). This trend is unusual because the sample displays re-entrant ordering when increased to 16 wt % (Figure 8d). This structure is easily identifiable as a BCC crystal because the twin structure gives a diffraction image with four diffraction spots in the innermost ring and spots occurring just vertical to the first four in the second ring. Finally, as shown in Figure 8f, the crystal melts for the last time at 20 wt %. We believe the melting observed at 20 wt % is consistent with the melting trend identified in the four previous systems investigated, making the first melting and the re-entrant crystallization a unique characteristic of the 36K/36K *d*-PS/PI system.

We can understand this conceptually by recalling that the micelles comprising 36K/36K/ *d*-PS/PI diblocks form micelles with a hydrodynamic radius of 467 Å and a core radius equaling 142 Å. This gives a ratio for the hydrodynamic coronal layer thickness to core radius ($\langle L \rangle_h / R_c$) of approximately 2.29. On the basis of this criteria, we conclude that the 36K/36K *d*-PS/PI micelles are the most diffuse, starlike, system studied in our investigations. Richter and co-workers speculated that star polymers should melt and display re-entrant ordering as the stars first disorder to a homogeneous sea of chains and then begin to feel the presence of the cores at more advanced concentrations.[37] Since our 36K/36K *d*-PS/PI micelles are the most starlike, we suspect this corresponds to the re-entrant ordering expected for star polymers. The second ordering transition is now observed at more modest concentrations than would be expected for true star polymers because the polymeric micelles have appreciable cores.

Although each diblock system displays some unique phase behavior as we increase the polymer concentration and approach melt conditions, we still discern some general trends in the scattering images. While some of these systems have a BCC cubic micellar structure and others display an FCC crystal, both types of crystals globally disorder, displaying isotropic scattering typical of a strongly correlated liquid even though this transition can take place at quite disparate concentrations ranging from 12 to 50 wt %. Secondly, the scattering from concentrations near the melt gives strongly anisotropic scattering images. While we are reticent to

describe this as diffraction, we can positively interpret this anisotropy as representing elongated structures associated with the melt. As a result, the anisotropy marks a region where shape transitions, first identified by Gallot, are located. Thus, we are left with a simple picture of the phase behavior of polymeric micelles that includes a disorder−order−disorder process as the micelle concentration is increased. Since the disordering takes place before the shape transitions are observed, this means we should be able to understand the order−disorder process in terms of the physical characteristics of these polymeric micelles.

3. Discussion

3.1. Understanding the High-Concentration Disordering of Polymeric Micelles. The experimental evidence for the disordering of polymeric micelles upon increasing the polymer concentration appears disparate at first glance. The self-consistent field (SCF) equations,[21,38] we used to model the interactions between polymeric micelles yields pair potentials that accurately describe the liquid structure[21] and the disorder−order transition.[27] These same interaction potentials predict a stable crystalline phase even at volume fractions where we observe the disordering process. In some sense, the loss of structure, regarded here as melting, can be viewed as a breakdown of the pair potentials. Predictions of the micellar structure based on these pair potentials will give ordered structures whose free energy and pressure becomes increasingly divergent as the micelles are compressed and the lattice shrinks upon increasing the micelle concentration. While it remains accurate to describe the structure in polymeric micelles with pair-interaction potentials developed from tethered-chain models, we must recognize that the physics of these tethered-chain systems regulates the phase behavior we observe experimentally.

We realize that the thermodynamics of concentrated polymer solutions is quite complicated. The simplest example involves homopolymers suspended in a good solvent, say polyisoprene in decane. Even for such a system, the thermodynamics are split into three regimes: dilute, semidilute, and concentrated.[39] In the dilute regime, the system behaves as individual swollen coils in a good solvent. The semidilute regime allows the polymers to interact with each other but the chains do not strongly overlap. For the concentrated regime, the polymers strongly overlap, and the effects of their neighbors produce a mean field similar to the melt. As a consequence, the pressure is reduced in the concentrated regime and the chains change from a swollen to a Gaussian conformation more closely associated with the melt. These seemingly subtle conformational changes dramatically influence the thermodynamics of polymeric suspensions. As a result, we can envision changes in the physics of these tethered-chain systems if we retain the micellar architecture and continue to shrink the lattice dimension causing the tethered chains to interact very strongly with their opposing layers.

In fact, Richter and co-workers[37] observed similar behavior in many-armed star polymers. Although they do not experience the same richness in phase behavior for star polymers as found in our polymeric micelles, they observe an interesting trend in the structure factor as they increase the star polymer concentration. At modest concentrations, the structure factor for stars of 18 and 64 arms shows the expected modulation as the polymer concentration is increased, namely an increase

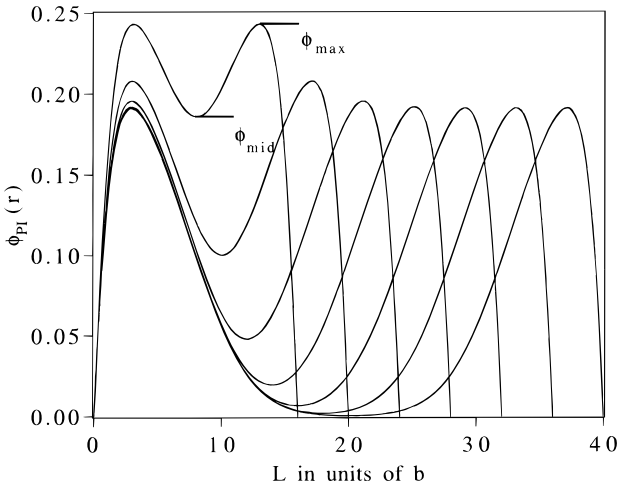

Figure 9. Polyisoprene density profiles between a pair of interacting 20K/10K *d*-PS/PI micelles in decane as a function of different surface to surface separations in terms of Kuhn lengths of the polyisoprene chain outlining the values of ϕ_{max} and ϕ_{mid}.

in the magnitude of the first peak in the structure factor. As they increase the concentration further, they begin to observe a loss in the correlation between star polymers identified by a systematic decrease in the first peak of the structure factor upon increasing the concentration. Because the cores of these star polymers are quite small, they attribute the loss in structure to exceeding the overlap concentration where the sample becomes a homogeneous sea of chains and so the positions of the cores become random.

While the work of Richter and co-workers lacks a quantitative model, their interpretation represents an important advance in understanding the physical properties of concentrated, strongly interacting tethered-chain systems. By analogy, we expect a similar trend in the behavior of our polymeric micelles. We return to the SCF equations used to predict the pair potentials and now examine changes in the density profiles explicitly.[21,38] In a manner identical to the method used to calculate the increase in free energy from the noninteracting state, we now investigate the density profiles of strongly interacting layers. Because we know the core curvature and surface density from dilute small-angle scattering experiments, we can hold a pair of micelles at a fixed separation and solve self-consistently for the density profiles of the interacting layers along the centerline in units of the Kuhn length for polyisoprene (b = 8.28 Å).[40,41] In Figure 9, we show the resulting polyisoprene density profiles for our 20K/10K *d*-PS/PI micelles at various surface-to-surface separations (L). Most notably, one notices that as the separation decreases, layers are forced to interdigitate or compress and the density profiles are augmented. In particular, the maximum local density increases as the layers are forced together. This can arise from either interdigitation or compression; a mean-field analysis prevents us from attributing this change to the detailed chain conformation. More importantly, we notice that the local polymer density at the midpoint changes significantly for these interacting layers. In fact, at close separations the density at the midpoint approaches that at the surface of the micelle. In physical terms, this local polymer gradient is responsible for the effective pair potential that drives the crystallization process. Conceptually, when the density profile is constant we lose the osmotic pressure gradient responsible for the

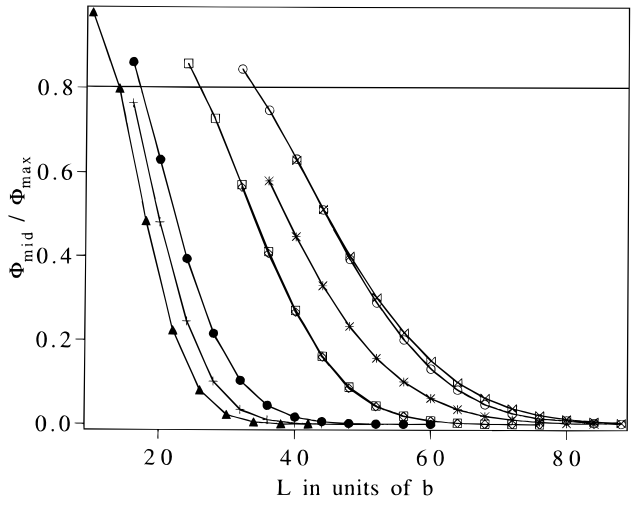

Figure 10. ϕ_{mid}/ϕ_{max} as a function of surface separation for our polymeric micelles. As this ratio approaches unity, the osmotic pressure gradient dissipates and induces the melting of our micellar crystals. We find that a value of $\phi_{mid}/\phi_{max} = 0.8$ describes the volume fractions for this order−disorder transition.

repulsive pair interaction potential and expect the micellar crystal to melt. In short, when the opposing layers are held at a separation where the density profile across the gap is constant, the chains adopt a more Gaussian conformation and are less influenced by the surface to which they are tethered. This eliminates the effective pair potential and causes the micellar crystal to melt.

One way to quantify this effect is by evaluating a ratio of the local polymer density at the midpoint relative to the maximum that occurs close to the core tethering surface for various surface separations. In this way we remove the variability in surface density for each micellar system and generate a relative comparison of the effective strength of the polyisoprene density gradient as a function of particle surface separation. Figure 10 shows this effective gradient plotted against the surface separation (L) for all of our micelles. As ϕ_{mid}/ϕ_{max} approaches unity, the density profile is constant, corresponding to almost no osmotic pressure gradient. As this ratio approaches zero, the gradient is maximized. Although we expect the melting process to occur when the density profile is constant, the profiles show an inflection for excessively close separations. Furthermore, this one-dimensional representation of interacting micelles is a simplification of all the interacting neighbors. For these reasons we concern ourselves with interpreting the melting of our micellar crystal as a function of a constant ratio of ϕ_{mid}/ϕ_{max} in order to describe the melting of our micellar crystals upon increasing the polymer concentration.

We can relate this critical surface-to-surface separation (L) to the volume fraction of polystyrene through the micellar core radius. The schematic in Figure 11 shows that this separation is related to the nearest-neighbor distance in the micellar crystal. Because of the differences in lattice geometries and packing densities, we arrive at the following expression for the polystyrene volume fraction of an FCC crystal in terms of the separation distance (L):

$$\Phi_{PS} = \frac{4\pi\sqrt{2}}{3}\left(\frac{R_c}{2R_c + L}\right)^3 \qquad (1)$$

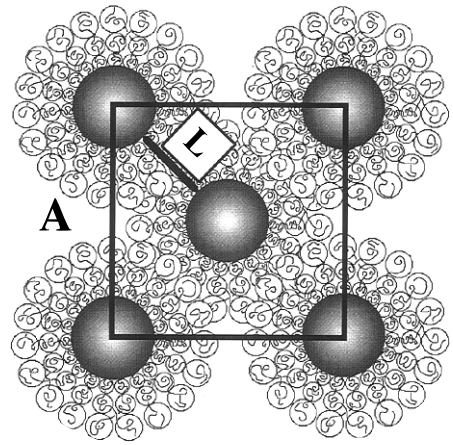

Figure 11. Schematic relating the critical volume fraction to the critical surface separation (L) through the nearest-neighbor distance for the appropriate lattice.

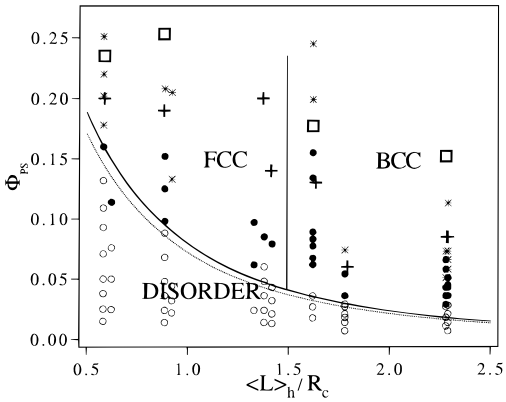

Figure 12. Semiquantitative phase diagram for our polymeric system detailing regions of liquid-like disorder (○) and crystalline order (●) as well as higher concentrations where the scattering is no longer consistent with the regionally specified lattice type (*). The coexistence curves estimate the freezing and melting volume fractions as a function of the hydrodynamic layer thickness to core radius ($\langle L\rangle_h/R_c$) based on previous work.[27] To this phase diagram, we add estimates of the melting process (+) as a consequence of the diminished osmotic pressure gradient and the onset of shape transitions (□).

and for the BCC lattice we arrive at

$$\Phi_{PS} = \pi\sqrt{3}\left(\frac{R_c}{2R_c + L}\right)^3 \qquad (2)$$

From this information we can choose values of constant ϕ_{mid}/ϕ_{max} and calculate the separation for each micellar crystal. Knowing the preferred lattice type for each crystal allows us to calculate the critical volume fraction where increasing the micellar concentration further would push the particles closer, causing them to melt. We find a value of $\phi_{mid}/\phi_{max} = 0.8$ provides reasonable agreement with our experimental data.

We return to the phase diagram reported in Figure 12, with the disorder−order process outlined with solid lines corresponding to the scaling relation developed in earlier work, to add our predictions of the order−disorder process, now elucidated by the larger (+) symbols. For the most part, this analysis provides a reasonable prediction of the seemingly disparate disordering process observed experimentally and denoted by the (*) symbols. The choice of a critical ratio ϕ_{mid}/ϕ_{max} only reflects the fact that the density profile in the gap is becoming homogeneous. Since this is a one-dimen-

sional picture of a three-dimensional system, we are not overly concerned with the use of a ratio below unity. Rather, we wish to emphasize that originally disparate melting phenomenon can be understood in terms of a single measure of the strength of the osmotic pressure gradient.

3.2. Anisotropy from Shape Transitions. The phase digram presented in the preceding section highlights the analogy between our polymeric micelles and colloidal systems, specifically, the disorder−order transition and the regions of FCC and BCC crystals that depend on the length scale of the repulsion. Of course this analogy fails with the onset of the melting process that develops as the concentration is increased. Even without this melting process, we anticipate limits for this colloidal analogy based on more general arguments about the phase behavior of concentrated diblock copolymer solutions. This limit can be understood conceptually by using the highly solvated micellar crystals as a reference state. As the micellar concentration increases, the lattice constant decreases and micelles are compressed together, effectively squeezing solvent out of the system. At some point all the solvent is removed and a melt diblock sample is left. Polystyrene/polyisoprene diblocks of this degree of polymerization exhibit ordered melt morphologies that include close-packed cylinders, lamellae, etc. Ultimately these diblock solutions must undergo shape transitions, disrupting the low concentration micellar architecture, to form structures closely resembling the melt morphology. Alternatively, this process can be understood using the melt morphology as the reference state. As modest quantities of solvent are added to the melt sample, the solvent may penetrate one or both domains depending on its selectively. Solvating one or both domains with modest quantities of solvent may not disrupt the macrolattice order, and so estimating the morphology based on an adjusted volume fraction is referred to as the dilution approximation. Recent work by Lodge and coworkers[42] has focused attention on the dilution approximation for diblock systems in the presence of small amounts of solvent. They determined that the dilution approximation can fail at surprisingly modest quantities of solvent owing to significant changes in the entropic contribution to the free energy associated with adding a small molecule. This effect may be especially dramatic in disrupting the macrolattice when the solvent can penetrate both domains (good solvents for both blocks).

While the solvated micellar crystals and melt morphologies represent convenient reference states because their ordered structures are well understood, it still remains a challenge to apply this knowledge to concentrations intermediate to these two states. Unfortunately, extending our knowledge from these two reference states to describe the phase behavior at intermediate concentrations poses formidable obstacles because concentration range is wide and the onset of shape transitions requires detailed information about the shape of the macromolecular assembly to specify the interactions between such assemblies. We have already taken advantage of the SCF models for micelles to qualitatively explain the melting process. In some sense, this represents the limit for the micellar crystals as a reference state.

At elevated concentrations as high as 85 wt %, we still do not observe sufficient diffraction peaks to fully characterize the ordered melt morphology. For example, the 45K/45K *d*-PS/PI system has an ordered melt morphology of lamellae where we expect equidistant diffraction spots along one direction. The lack of higher order diffraction spots prevents us from conclusively identifying this sample as lamellar. Recent work by Hammouda and Balsara[43] on 11K/17K PS/PI diblocks in dioctyl phthalate (a good solvent for both blocks) at a concentration of 65 wt % interpreted their anisotropic scattering as diffraction from lamellar structures. Without the conclusive evidence of higher order diffraction spots, we reserve our judgement about the possible reordering of the 45K/45K *d*-PS/PI diblocks at near melt conditions presented in this work. Due to Lodge and co-workers' finding of the failure of the dilution approximation,[42] we cannot apply the dilution approximation and use the melt condition as a reference state. We are confident that this scattering anisotropy corresponds to a lamellar-like sample forming elongated structures with essentially equal spacing along the vorticity direction. As a result, the scattering anisotropy observed in these experiments offers a transition point in each system marking the destruction of micellar architecture observed at lower concentrations. The scattering from these samples at concentrations intermediate to the melt and micellar crystals shows line broadening apparent in the radial averages as well as an anisotropy that allows a reasonable estimate of the onset of these shape transitions.

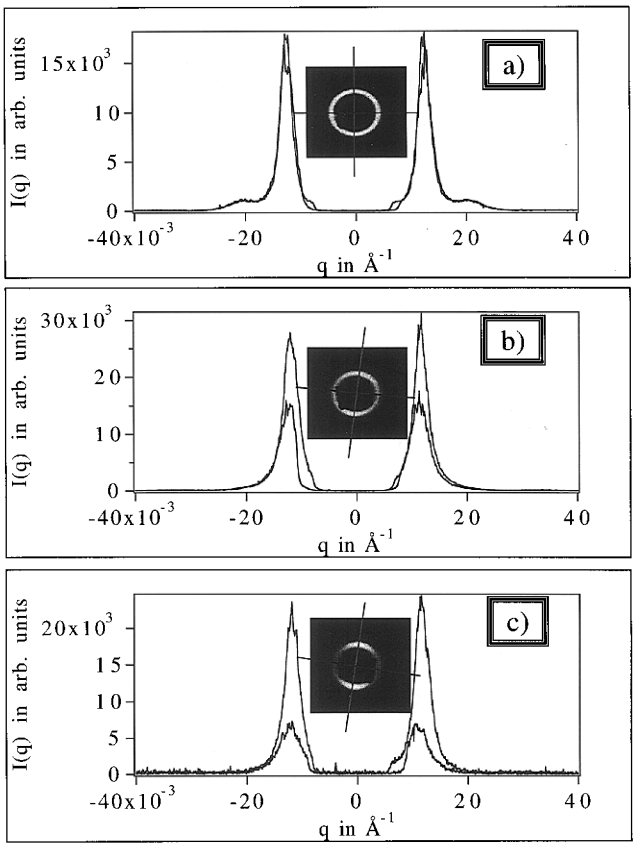

Figure 13. Determination of scattering anisotropy for 45K/45K *d*-PS/PI diblocks in decane at the following concentrations: (a) 30, (b) 50 and (c) 70 wt %.

One way to quantify this anisotropy is by choosing a pair of orthogonal lines along the directions of minimum and maximum intensity for comparison. Figure 13 shows a comparison of this scattering anisotropy for the 45K/45K *d*-PS/PI system at concentrations of 30, 50, and 70 wt %. For the 30 wt % sample the ring is essentially isotropic and so the two curves overlap. At 50 wt %,

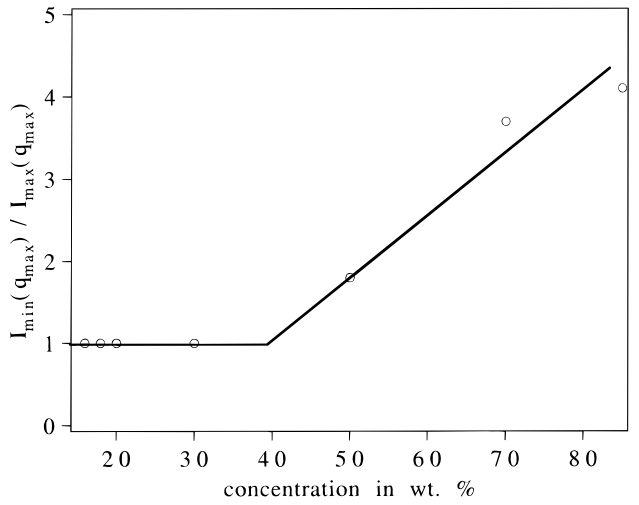

Figure 14. Plot of anisotropy factor as a function of total polymer concentration for 45K/45K *d*-PS/PI diblocks in decane.

we see that the two curves do not overlap and the ratio of the maximum intensity along the vertical direction is almost twice that along the orthogonal direction. By 70 wt %, the scattering anisotropy is even more dramatic with a ratio of almost 4 between the maxima along these two directions. The strong anisotropy is compelling evidence for highly aligned structures. Plotting this intensity asymmetry as a function of concentration allows us to estimate where shape transitions first develop. This ratio should diverge as one obtains diffraction from ordered lamellae. Figure 14 shows this result for our 45K/45K *d*-PS/PI system. In practice, we cannot extend this analysis to lower concentrations because the micellar crystals also exhibit anisotropic scattering. Since these micelles first melt before the shape transitions, tracing a change in the anisotropy provides a convenient way of estimating the concentration where shape transitions occur. For the 45K/45K *d*-PS/PI system, a concentration of almost 40 wt % marks the shift from isotropic to anisotropic scattering. We can also use considerations about the line broadening in the radial averages to aid in our determination. Given this estimate for the onset of shape transitions, we now add this specification to our phase diagram (Figure 12). The (*) symbols correspond to samples that exhibit a loss of order with the regionally specified lattice type. The (□) symbol corresponds to our estimates of the onset of the shape transitions for select systems.

4. Conclusion

We set out to study the inevitable shape transitions occurring when a concentrated suspension of polymeric micelles approaches melt conditions. We found a curious melting transition preceding the onset of scattering anisotropy. We observed a general mechanism for the transition from cubic micellar crystals to the more general structures. The mechanism first involves the melting of the cubic crystal resulting in a disorder−order−disorder transition for all of our polymeric micelles. The initial disorder−order transition is elucidated by developing pair-interaction potentials from SCF theories for chains tethered to spherical cores and using statistical mechanical models for simple fluids.[27] These models predict the formation of a stable crystalline phase that is preserved upon increasing the micellar concentration although the pressure diverges as the particles are forced closer together on their lattice. Appealing to these same SCF models, we can understand the order−disorder process as occurring at a point where the tethered chain density becomes relatively constant across the gap, removing the osmotic pressure gradient that drives the pair potential and causing the micellar crystal to melt in a manner analogous to the loss in correlations observed upon increasing the concentration of star polymers. One system exhibits a reentrant transition, melting initially and then reordering as the influence of the concentrated region around the core becomes important. This occurs in the most diffuse, starlike micelle; it undergoes *disorder−order−disorder−order−disorder* transitions as the concentration increases.

In studying the phase behavior of these concentrated diblock copolymer solutions, we encountered a number of experimental limitations. The lack of temperature variability for the shearing device prevented us from examining samples asymptotically close to the melt. If we could raise the temperature nearer to the glass transition for polystyrene, we could more easily shear the concentrated diblocks when the polystyrene is the major phase. Although the rectangular shearing device required very small sample sizes, the inability to probe directions both parallel and perpendicular to the shear gradient limits our ability to identify the concentration where the melt morphology begins. SAXS diffraction using a couette with temperature variability would provide a more suitable arrangement for such investigations. Despite these limitations, the anisotropy in the scattering of the concentrated solutions allowed us to infer the onset of shape transitions, marking the loss of micellar architecture.

In summary, we conclude that the pair potentials that predict the disorder−order transition dramatically underscore the way polymeric micelles are inherently colloidal, while the order−disorder transition highlights their polymeric nature. The SCF framework for tethered-chain systems provides a link between these two approaches (colloidal and polymeric), allowing accurate insights into the unique behavior of polymeric micelles.

Acknowledgment. We acknowledge the support of the Stanford Synchrotron Radiation Laboratory in providing the facilities used in this experiment. The operation of the Stanford Synchrotron Radiation Laboratory is supported by the Department of Energy (DOE), Office of Basic Energy Sciences, Divisions of Chemical and Material Sciences. We wish to thank Hiro Tsuruta for coordinating the installment and assisting in the commissioning of the CCD detector at Beamline 1-4. We are especially indebted to Eric K. Lin for performing the SCF calculations used in this investigation. We also thank Steven D. Smith of Procter & Gamble for generously donating the polymers used in these experiments. This work was supported by the MRSEC Program of the National Science Foundation under Award No. DMR-9400354.

References and Notes

(1) Bates, F. S. *Science* **1991**, *251*, 898.
(2) Koppi, K.; Tirrell, M.; Bates, F. *Phys. Rev. Lett.* **1993**, *70*, 1449.
(3) Koppi, K.; Tirrell, M.; Bates, F.; Almdal, K.; Colby, R. *J. Phys. II Fr.* **1992**, *2*, 1941.
(4) Hadziioannou, G.; Skoulios, A. *Macromolecules* **1982**, *15*, 258.
(5) Sakurai, S.; Momii, T.; Taie, K.; Shibayama, M.; Nomura, S.; Hashimoto, T. *Macromolecules* **1993**, *26*, 485.

(6) Hashimoto, T.; Kawamura, T.; Harada, M.; Tanaka, H. *Macromolecules* **1994**, *27*, 3063.
(7) Almdal, K.; Koppi, K.; Bates, F. *Macromolecules* **1993**, *26*, 4058.
(8) Hajduk, D.; Harper, P.; Harper, S.; Honeker, C.; Kim, G.; Thomas, E.; Fetters, L. *Macromolecules* **1994**, *27*, 4063.
(9) Hajduk, D.; Harper, P.; Gruner, S.; Honeker, C.; Thomas, E.; Fetters, L. *Macromolecules* **1995**, *28*, 2570.
(10) Leibler, L. *Macromolecules* **1980**, *13*, 1602.
(11) Kinning, D.; Thomas, E.; Fetters, L. *J. Chem. Phys.* **1989**, *90*, 5806.
(12) Bates, F. S.; Berney, C.; Cohen, R. *Macromolecules* **1983**, *16*, 1101.
(13) Kao, C.; de la Cruz, M. *J. Chem. Phys.* **1990**, *93*, 8284.
(14) Shibayama, M.; Hashimoto, T.; Hasegawa, H.; Kawai, H. *Macromolecules* **1983**, *16*, 16.
(15) Hashimoto, T.; Shibayama, M.; Kawai, H.; Watanabe, H.; Kotaka, T. *Macromolecules* **1983**, *16*, 361.
(16) Shibayama, M.; Hashimoto, T.; Hasegawa, H.; Kawai, H. *Macromolecules* **1983**, *16*, 1427.
(17) Hashimoto, T.; Shibayama, M.; Kawai, H. *Macromolecules* **1983**, *16*, 1093.
(18) Shibayama, M.; Hashimoto, T.; Kawai, H. *Macromolecules* **1983**, *16*, 1434.
(19) Halperin, A.; Tirrell, M.; Lodge, T. P. *Adv. Polym. Sci.* **1992**, *100*, 31.
(20) McConnell, G. A.; Gast, A. P.; Huang, J. S.; Smith, S. D. *Phys. Rev. Lett.* **1993**, *71*, 2102.
(21) McConnell, G. A.; Lin, E. K.; Gast, A. P.; Huang, J. S.; Lin, M. Y.; Smith, S. D. *Faraday Discuss.* **1994**, *98*, 121.
(22) Milner, S. T. *Science* **1991**, *251*, 905.
(23) Dolan, A. K.; Edwards, S. F. *Proc. R. Soc. London, A* **1975**, *343*, 427.
(24) Dolan, A. K.; Edwards, S. F. *Proc. R. Soc. London, A* **1974**, *337*, 509.
(25) Edwards, S. F. *Proc. Phys. Soc.* **1965**, *85*, 613.
(26) Dan, N.; Tirrell, M. *Macromolecules* **1992**, *25*, 2891.
(27) McConnell, G. A.; Gast, A. P. Predicting Disorder−Order Phase Transitions in Polymeric Micelles. *Phys. Rev. E* **1996**, *54*, 5447.
(28) Gallot, B. *Adv. Polym. Sci.* **1978**, *29*, 87.
(29) Douy, A.; Gallot, B. *Mol. Cryst. Liq. Cryst.* **1971**, *14*, 191.
(30) Smith, S. D. In *Polymer Solutions, Blends, and Interfaces*; Noda, I., Rubingh, D. N., Eds.; Elsevier: New York, 1992; pp 43−64.
(31) Russell, T. P. In *Handbook of Synchrotron Radiation*; Brown, G., Moncton, D., Eds.; North-Holland: Amsterdam, 1991; Vol. 3.
(32) McConnell, G. A.; Lin, M. Y.; Gast, A. P. *Macromolecules* **1995**, *28*, 6754.
(33) Plano, R.; Safinya, C.; Sirota, E.; Wenzel, L. *Rev. Sci. Instrum.* **1993**, *64*, 1309.
(34) Safinya, C.; Sirota, E.; Bruinsma, R.; Jeppesen, C.; Plano, R.; Wenzel, L. *Science* **1993**, *261*, 588.
(35) Stanton, M.; Phillips, W. C.; O'Mara, D.; Naday, I.; Westbrook, E. *Nucl. Instrum. Methods Phys. Res. A* **1993**, *325*, 558.
(36) McConnell, G. A. Structure and Interactions in Concentrated Diblock Copolymer Solutions, Ph.D. Thesis, Stanford University, 1996.
(37) Richter, D.; Jucknischke, O.; Willner, L.; Fetters, L.; Lin, M.; Huang, J.; Roovers, J.; Toporovski, C.; Zhou, L. *J. Phys. IV* **1993**, *3*, 3.
(38) Lin, E. K.; Gast, A. P. *Macromolecules* **1996**, *29*, 390.
(39) Doi, M.; Edwards, S. *The Theory of Polymer Dynamics*; Clarendon Press: Oxford, 1986.
(40) Brandrup, J.; Immergut, E. H. *Polymer Handbook*, 3rd ed.; John Wiley & Sons: New York, 1989.
(41) Bauer, B. J.; Fetters, L. J.; Graessley, W. W.; Hadjichristidis, N.; Quack, G. F. *Macromolecules* **1989**, *22*, 2337.
(42) Lodge, T.; Pan, C.; Jin, X.; Liu, Z.; Zhao, J.; Maurer, W.; Bates, F. *J. Polym. Sci., Part B* **1995**, *33*, 2289.
(43) Balsara, N.; Hammouda, B. *Phys. Rev. Lett.* **1994**, *72*, 360.

MA961241N